Effect of Carbon and Nitrogen content on deformation and fracture of AISI 304 austenitic stainless steel

A. Molinari, M. Composta, C. Menapace
Department of Materials Engineering and Industrial Technologies, University of Trento (Italy)

RIASSUNTO. In questo lavoro è stato studiato l'effetto di modeste differenze nel contenuto di carbonio e di azoto sulla deformazione e il comportamento a frattura a temperatura ambiente di un acciaio inossidabile austenitico AISI 304. Nell'acciaio contenente il più basso contenuto degli elementi interstiziali si forma una maggiore quantità di martensite indotta dalla deformazione plastica dell'austenite; ne risulta un aumento dell'incrudimento, della deformazione uniforme e della deformazione totale. La presenza di aree martensitiche di dimensioni significative nella sezione resistente causa però localizzazione della deformazione all'interfaccia austenite/martensite, e questo promuove la nucleazione di cricche e la loro propagazione all'interfaccia stesso. Questo fenomeno determina una diminuzione di UTS. La trasformazione martensitica indotta dalla deformazione causa inoltre una diminuzione della "strain rate sensitivity".

ABSTRACT. The effect of small differences in the content of carbon and nitrogen on the room temperature tensile deformation and fracture behaviour of an AISI 304 stainless steel was studied. In the steel containing the lower amount of carbon and nitrogen, a higher amount of strain induced α' martensite is formed, which increases strain hardening rate and both uniform and total elongation at fracture. The presence of large martensitic areas in the cross section causes strain localization at the austenite/martensite interface, which promotes the nucleation of cracks and their propagation along the interface. This results in a decrease of Ultimate Tensile Strength. Strain induced transformation slightly reduces strain rate sensitivity, as well.

KEYWORDS: Strain induced transformation; stainless steel; plastic deformation; fracture

1 INTRODUCTION

The mechanisms responsible for plastic deformation of austenitic stainless steel depend on the Stacking Fault Energy SFE. On decreasing SFE, plasticity is provided by gliding of partial and perfect dislocations, gliding and mechanical twinning, gliding and strain induced martensite formation, which results in different elongation, strain hardening and strain hardening rate [1]. SFE depends on temperature, grain size and chemical composition. It decreases with decreasing temperature [2] and increasing grain size [3], whilst the effect of chemical composition depends on the specific element and, in some cases, on its amount, as reported by several authors [3, 4, 5, 6]. Among alloying elements, interstitial carbon and nitrogen are the most effective strengtheners, having a significant effect on yield strength even when restricted within the ranges allowed by international standards for conventional AISI304 and AISI316 stainless steels. Concerning the effect on plastic deformation mechanisms, whilst carbon increases SFE [1], the effect of nitrogen is not yet clarified and doubts still exist as to whether it increases or decreases SFE [7, 8, 9, 10].

In our work we studied the effect of small differences in carbon and nitrogen content on the deformation and fracture behaviour of an AISI 304 stainless steel. The study was based on tensile tests, carried out at room temperature with different strain rates, on the analysis of the true stress-true strain diagrams and on the analysis of the fracture surface.

2 EXPERIMENTAL PROCEDURE

The chemical composition of the two AISI 304 stainless steels is shown in Tab. 1.

The microstructure analysis was carried out using a Light Optical Microscope (LOM): two different etching procedures were adopted:

1. electrolytic etching in a 10% oxalic acid in distilled water solution, to reveal the as rolled microstructure;
2. chemical etching in a 40 ml HCl, 60 ml C_2H_5OH, 2 g $CuCl_2$ solution to reveal martensite.

The volumetric percent of martensite/ferrite was measu-

red by X-Ray Diffractometry (XRD), using the CuKα radiation and a monochromator on the diffracted beam.
The specimens for tensile tests were machined from the sheets along the three main directions (longitudinal, transverse and at 45° with respect to the rolling direction) according to ASTM E8M-04. Five specimens from each direction were obtained.
Tensile tests were carried out on an Instron machine at three strain rates: 3 mm/min, 8 mm/min and 15 mm/min.
We then subjected the fractured tensile specimens to XRD analysis, to measure the martensite content, and observed the fracture surface at the Scanning Electron Microscope (SEM) to investigate the fracture mechanisms.

3 RESULT AND DISCUSSION

Microstructure and microhardness

Fig. 1 shows, as an example, the microstructure of steel A, comprising equiaxed austenitic grains (size 8 ASTM) with annealing twins. At higher magnification (Fig. 2), some delta ferrite strips can also be seen. The volumetric content of delta ferrite was measured by XRD obtaining 0.9% and 8% in steels A and C, respectively. The higher amount in steel C can be correlated to the lower carbon and nitrogen content. Neither LOM nor SEM analysis showed any carbide precipitation.
Microhardness is the same for both steels, 219 $HV_{0.05}$ and 222 $HV_{0.05}$, and corresponds to expected values for an AISI 304 hot rolled sheet.

Tensile properties

Tab. 2 reports the results of tensile tests carried out at 3 mm/min strain rate, averaged over the three directions. Steel A has a slightly higher yield strength, which can be correlated to the higher content of carbon and nitrogen; it also has higher Ultimate Tensile Strength and lower elongation (both uniform and total) than steel C.

Microstructure evolution on plastic straining

Figs 3 and 4 show the microstructure of steel A and C, respectively, close to the fracture surface. The presence of strain induced α' martensite is clearly evident, in particular in steel C. The content was measured by XRD. As previously mentioned, the as rolled specimens contain low percentages of delta ferrite, which has a bcc lattice very similar to that of α' martensite. The two XRD patterns cannot be distinguished by XRD. Then we calculated the content of martensite in the fractured

Steel	% C	% Si	% Mn	% P	% S	% Cr	% Ni	% Mo	% N
A	0.05	0.39	1.19	0.029	0.001	18.1	9.1	0.14	0.048
C	0.039	0.33	1.20	0.028	0.001	18.15	9.05	0.15	0.028

Table 1: Chemical composition of the investigated steels.

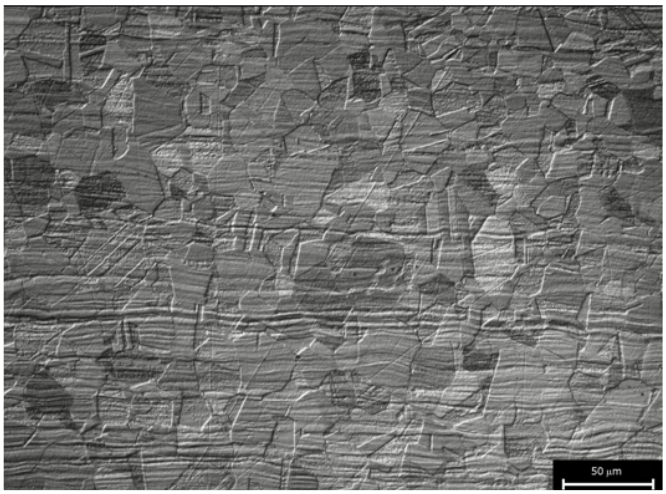

Figure 1. Microstructure of the as rolled AISI304 steel.

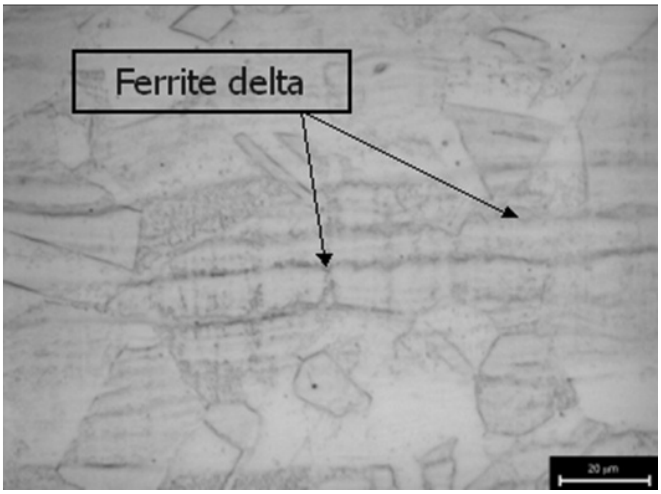

Figure 2. Detail of the microstructure of the as rolled AISI304 steel showing δ ferrite

Steel	$\sigma_{y0.2}$ (MPa)	ε_U %	UTS (MPa)	ε_B%
A	278.9 ± 3.33	65.6 ± 4.39	640.6 ± 9.9	73.5 ± 4.0
C	262.6 ± 3.8	69.6 ± 3.2	626.7 ± 12.8	76.4 ± 3.6

Table 2. Results of tensile tests at 3 mm/min.

specimens, subtracting the content of delta ferrite, which remains constant on straining, from the total amount of b.c.c. phase measured. The results are reported in Tab. 3. The higher amount of strain induced α' martensite in steel C can be attributed to the lower content of interstitials. Carbon and nitrogen decrease the athermal martensite transformation temperature (M_s) thus stabilizing austenite. However, whilst carbon increases SFE, thus reducing the possibility of formation of strain induced martensite, the effect of nitrogen is not well established, as previously mentioned. M_{D30} is the temperature (higher than M_s) at which 50% martensite is induced by a true tensile strain of 0.3. This temperature was calculated from the chemical composition according to the relation [11]

$$M_{D30}\,(°C) = 413\text{-}462(\%C+\%N)\text{-}9.2(\%Si)–8.1(\%Mn)–13.7(\%Cr)–9.5(\%Ni)–18.5(\%Mo) \quad (1)$$

obtaining 17.5°C and 32.1°C for steel A and C, respectively. Despite the discrepancy between M_{D30} as calculated and the amount of martensite measured in tensile specimens (in steel C, for instance, a total tensile strain of 0.76 at room temperature induces the formation of about 20% martensite, which is lower than that resulting from the definition of M_{D30}) the lower temperature for steel A with respect to C agrees with the greater amount of strain induced martensite in the latter type steel.

The microhardness of austenite was measured close to the fracture surface. The data is shown in Tab. 4. It is quite interesting to note that austenite is significantly harder in steel A, i.e. in the material which forms the lower amount of martensite. Since the microhardness increase is the result of strain hardening, these results can confirm that the response of austenite to mechanical loading is mainly governed by linear and surface defects in steel A and by the formation of martensite in steel C.

The effect of plastic strain on the strain induced transformation was investigated in steel C by measuring the amount of martensite at different strain levels. In steel A the total amount of martensite is too low to offer reliable information. The result is shown in Fig. 5: the transformation starts at about 0.25 strain and saturates at 23%, within the uniform deformation range. The dependence on strain follows a sigmoid trend. The reason for this behaviour lies in the mechanism for nucleation of strain induced martensite, as explained by several authors [12, 13, 14]: it nucleates in highly defective zones of austenite, as embryos confined to intersections of micro-shear bands which are composed of irregular, overlapping arrays of stacking faults and twins. A minimum amount of strain is then necessary to form such a defective volume, before α' martensite nucleates.

Strain hardening

Fig. 6 is the true stress - true strain curve of steel A in a log-log plot. It shows the typical behaviour of austenitic steels which is not characterized by a straight line (Ludwick-Hollomon model), but shows a progressive increase in the slope of the curve.

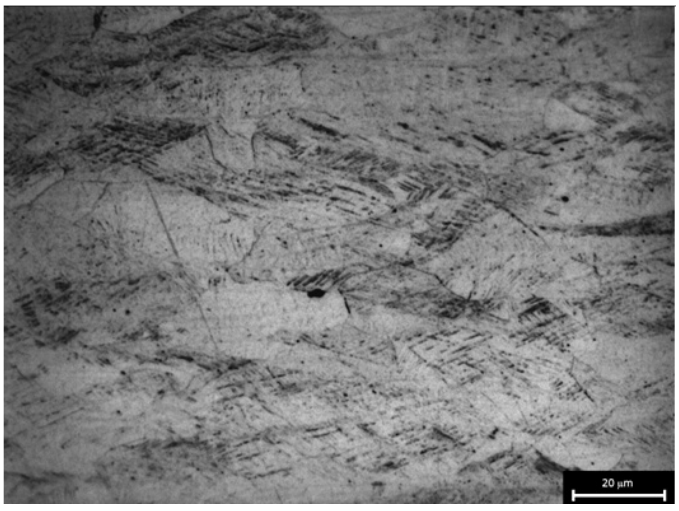

Figure 3. Strain induced martensite in steel A.

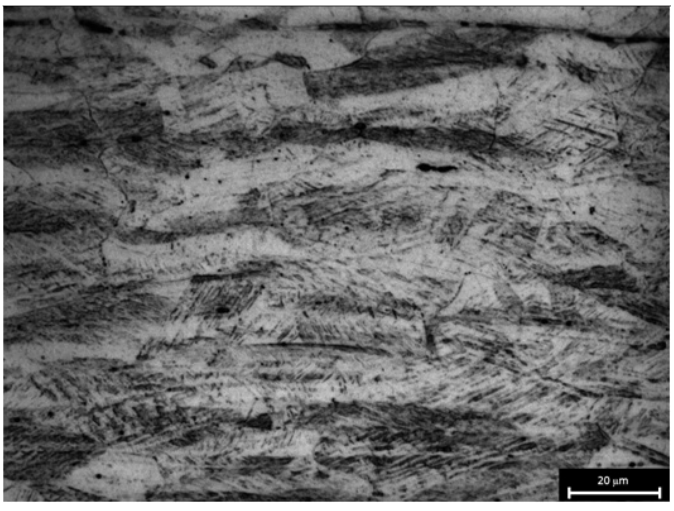

Figure 4: Strain induced martensite in steel C.

Steel	Martensite (+ δ-ferrite) volume percent	
	before strain	after strain (close to the fracture surface)
A	0 (+ 0.9)	2.1 (+ 0.9)
C	0 (+ 8)	23.6 (+8)

Table 3. Volumetric percent of strain induced martensite and ferrite as determined by XRD.

STEEL A	STEEL C
387.2 ± 9.1	359.2 ± 21.1

Table 4. Microhardness ($HV_{0.05}$) of strain hardened austenite.

The curve was then interpolated according to the model proposed by [15] for a stable austenite. The true stress - true strain relation is

$$\sigma = K\varepsilon^{(n_1+n_2\ln\varepsilon)} \quad (2)$$

where K, n_1 and n_2 depend on the steel, its structural state and deformation conditions. This equation was proposed by the authors as a simplified model with respect to that proposed by Ludwigson [16] to describe the flow curves which are concave upwards on logarithmic coordinates.

Fig. 7 shows that the theoretical curve fits quite well the experimental data (the straight line representing the Ludwick-Hollomon model is drawn, for comparison). From the interpolation of the curves of the two steels investigated, the parameters k, n_1 and n_2 were calculated and are shown in Tab. 5 along with R^2. The correlation coefficient is very good in both cases, and the slightly better value obtained for steel A can be correlated with its higher stability against strain induced transformation, since the model used is valid for a stable austenite.

As far as metastable austenite is concerned, Ludwigson and Berger [17] proposed a model which considers the contribution from strain hardening of austenite, strain induced transformation to martensite and strength of martensite to describe the flow curve of metastable austenitic steels. According to this model, an increase in nitrogen and carbon content is expected to increase $\sigma_{y0.2}$ and to decrease the ease with which austenite may transform to strain induced martensite, as actually verified in this study. At the same time, the increase in the interstitials content should result in an increase in elongation and a decrease of UTS, which does not agree with the

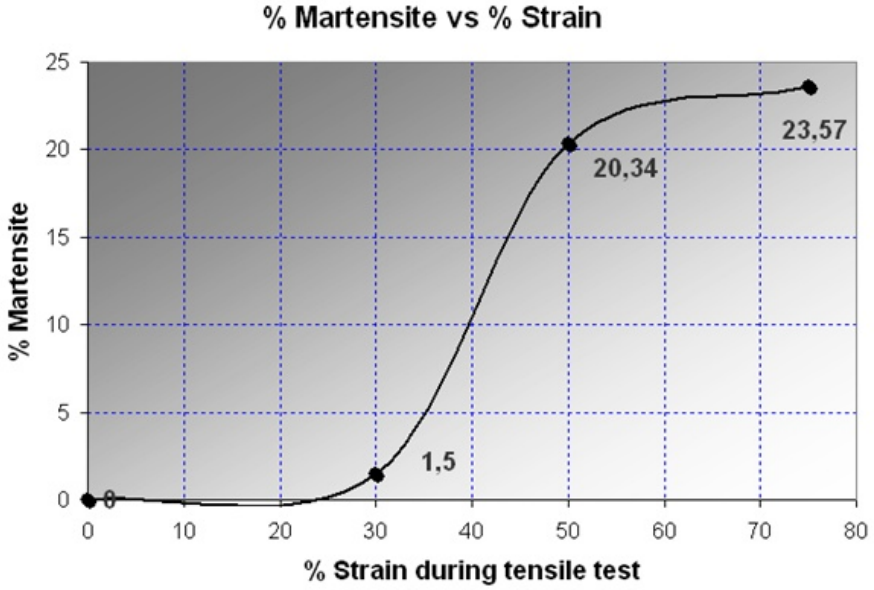

Figure 5. Amount of strain induced martensite versus plastic strain in steel C .

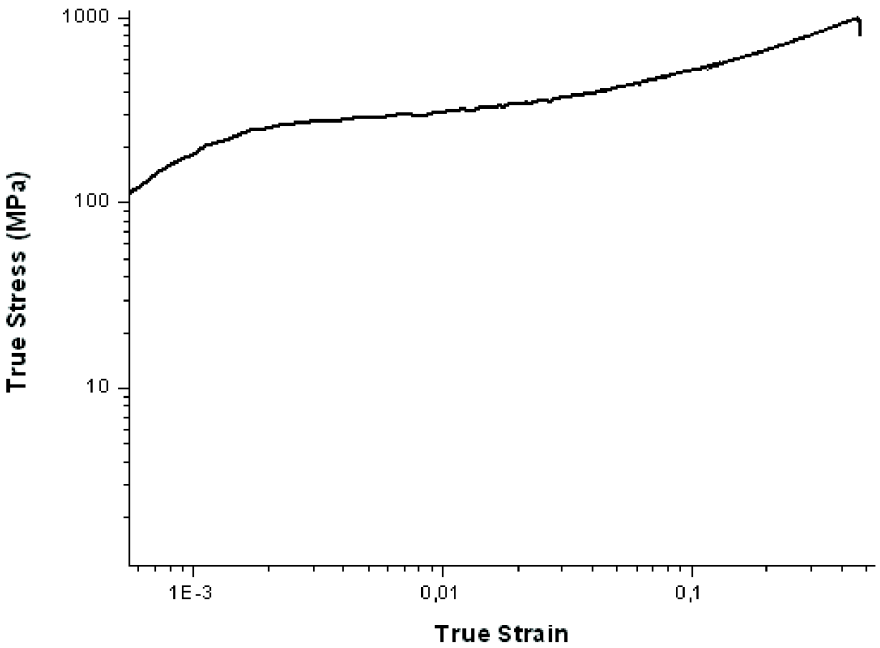

Figure 6. True stress – true strain curve of steel A.

results of our investigation. Therefore, the model proposed by Kim and Lim [18] was applied. The correlation between true stress and true strain is:

$$\ln\sigma = a(\ln\varepsilon)^2 + b(\ln\varepsilon) + c \quad (3)$$

where a, b and c are constants to be determined by interpolation of experimental data; the strain hardening rate is

$$n = \frac{d\ln\sigma}{d\ln\varepsilon} = M\varepsilon + N \quad (4)$$

where M and N are temperature dependent constants. Combining the above two equations results in the final equation

$$\sigma = K\varepsilon^N e^{(M\varepsilon)} \quad (5)$$

K is a constant depending on the material, whilst M describes how the flow stress increases with the plastic strain because of the strain induced transformation of austenite.

Fig. 8 compares the experimental and theoretical curves for steel A, and Tab. 6 lists the parameters of equation (5) for both steels. As can be expected from the different amount of strain induced transformation, M is higher in steel C than in A. Moreover, the correlation coefficient is very close to unity in both cases, but it is slightly higher for the less stable steel C.

Using data shown in Tab. 6, the strain hardening rate was calculated according to equation (4), and the results are in Fig. 9. The strain hardening rate increases with plastic strain quite similarly in the two steels. At about 0.25 strain, i.e. the strain at which strain induced transformation starts, the strain hardening rate of steel C be-

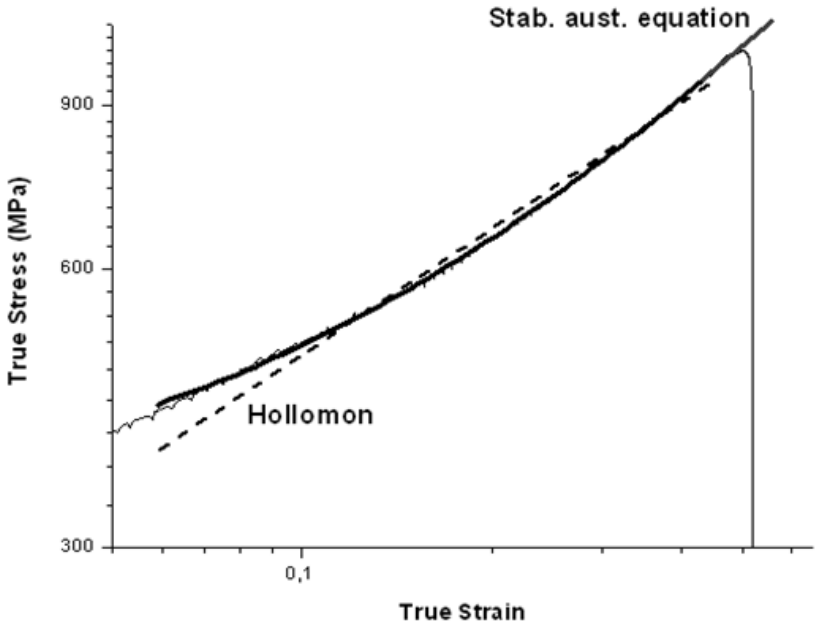

Figure 7. Interpolation of the plastic step according to a model for stable austenites, compared to the Ludwick-Hollomon model.

Steel	k	n_1	n_2	R^2
A	1587.84865 ± 15.02425	0.64990 ± 0.01300	0.07351 ± 0.00008	0.99992 ± 0.00001
C	1635.63372 ± 2.40758	0.70995 ± 0.00218	0.08187 ± 0.00112	0.99982 ± 0.00002

Table 5. Results of the interpolation of the plastic step of the true stress – true strain curves according to a model for stable austenite.

Steel	K	N	M	R^2
A	878.7071 ± 1.784243	0.2633 ± 0.02291	0.70185 ± 0.028214	0.99954 ± 7.0711E-05
C	773.0959 ± 33.77679	0.23955 ± 0.032315	0.86055 ± 0.079267	0.99973 ± 7.0711E-06

Table 6. Results of the interpolation of the plastic step of the true stress – true strain curves according to a model for metastable austenite.

comes higher than that of steel A, and the difference further increases with strain. Strain induced transformation in steel C results in an increase of the resistance of the steel to plastic flow, confirming results by Lebedev and Kosarchuk [19] who conclude that the greater the stability of austenite, the lower the strain hardening rate, and by A. K. De et al. [20]. Moreover, Spencer et al. [21] demonstrated that work hardening of AISI316L stainless steel increases with the strain induced transformation, provided that transformation does not reach completion at small strains (as in our work). In this case, strain induced transformation results in an increase in ductility, according to a TRansformation Induced Plasticity TRIP mechanism, as we actually found in this work.

Strain rate sensitivity

Tab. 7 reports the strain rate sensitivity m and the non uniform deformation of the two steels. Negative strain rate sensitivity implies low resistance to strain localization, which results in a low non uniform deformation [22]. Steel C has a more negative m, which means that the strain induced transformation has a negative effect on the resistance to localized straining.

Fracture behaviour

Figs. 10 and 11 show the fracture surfaces of the two steels. In steel A (Fig. 10) fracture is predominantly ductile, with the typical dimpled morphology; some macro voids are present, mainly localized in the central zone of the fracture surface. These macrovoids are more

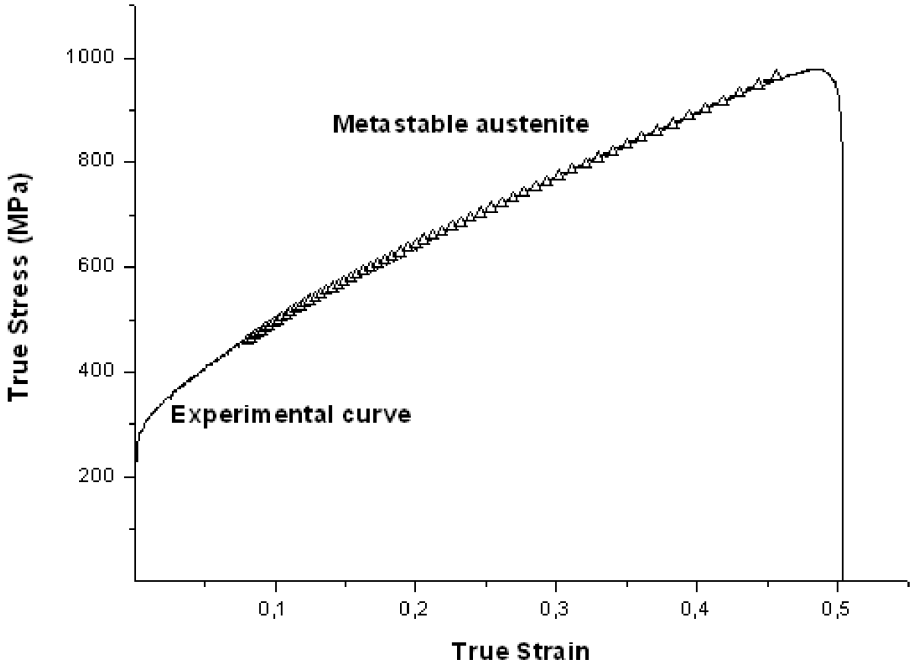

Figure 8. Interpolation of the plastic step according to a model for metastable austenites.

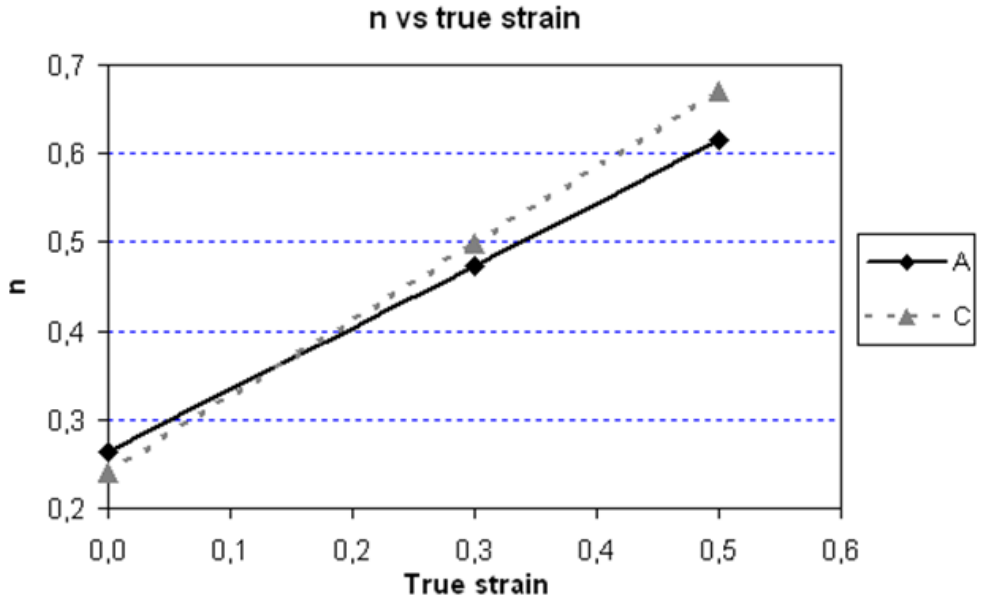

Figure 9. Strain hardening rate versus true strain.

numerous and larger in steel C (Fig 11), and the dimpled morphology is not yet the main feature of the fracture surface. The internal surface of macrovoids, when observed at higher magnification (Fig. 12), shows some fine striations, similar to deformation bands, which have been associated to strain induced transformation in an fcc Co alloy [23]. The size of macrovoids is comparable to that of the strain induced martensitic areas (20-40 μm in steel C, 5-10 μm in steel A).

The correlation between macrovoids and martensite is clear, and their formation can be attributed to interfacial separation between austenitic and martensitic areas, caused by nucleation and propagation of cracks induced by a large local strain in austenite close to the interface. The lower UTS of steel C with respect to steel A can then be correlated to the occurrence of this particular damage phenomenon associated with the presence of strain induced α' martensite.

4 CONCLUSIONS

Differing concentrations of interstitial elements in two AISI 304 austenitic stainless steels have a significant

Steel	ε_u	ε_r	$\varepsilon_r - \varepsilon_u$	m
A	0.656 ± 0.043	0.7349 ± 0.040	0.0788	-0.010 ± 0.003
C	0.6957 ± 0.032	0.7644 ± 0.036	0.0687	-0.020 ± 0.002

Table 7. Uniform deformation (ε_U) and total deformation (ε_R) at 3 mm/min; strain rate sensitivity measured at 3 and 15 mm/min.

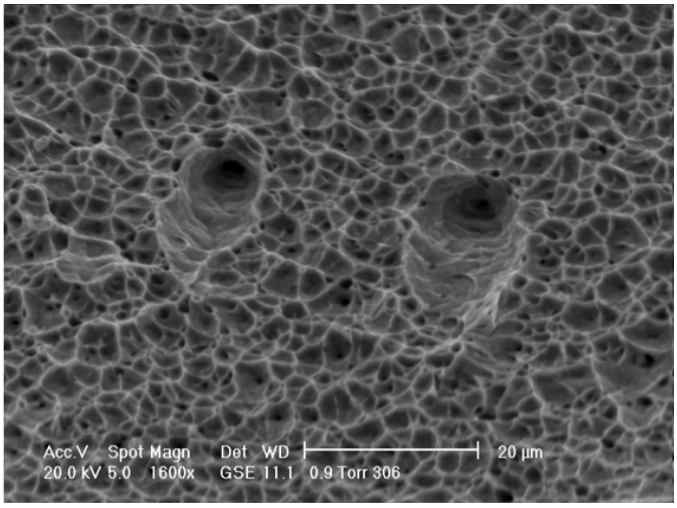

Figure 10. Fracture surface of steel A.

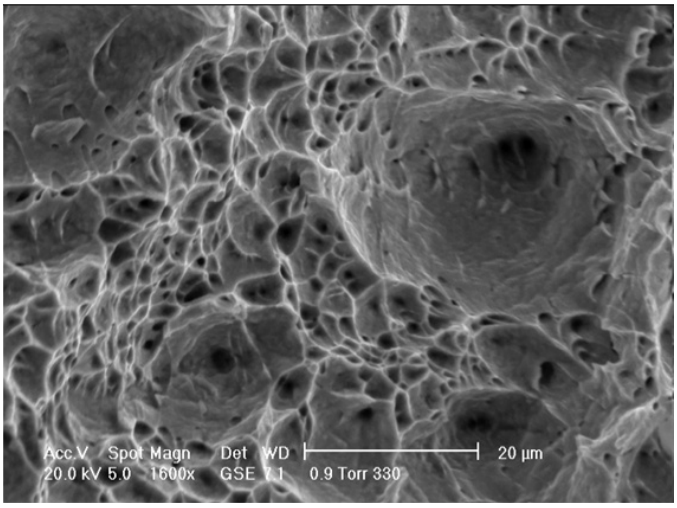

Figure 11. Fracture surface of steel C.

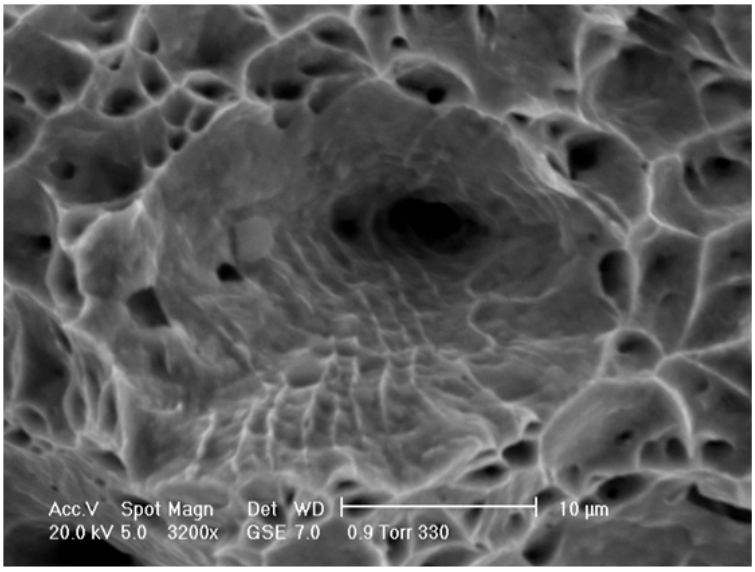

Figure 12. Detail of the macrovoids in the fracture surface of steel C.

influence on the plastic deformation and fracture behaviour under tensile loading of the steels. We attribute this to the differing stability of austenite towards strain induced martensite transformation.

In the steel containing the lower amount of carbon and nitrogen, a higher amount of α' martensite is formed during plastic straining, which increases the strain hardening rate, as determined by the analysis of the true stress-true strain curve, and the tensile elongation (TRIP). Moreover, the presence of large martensite areas in the cross section causes strain localization at the austenite/martensite interface, which promotes the nucleation of cracks and their propagation along the interface. This results in a decrease of Ultimate Tensile Strength. Strain induced transformation slightly reduces strain rate sensitivity as well.

Based on the combined effect on strain hardening and plasticity, the influence of small differences in carbon and nitrogen concentrations on tensile properties has been explained. On increasing the content of the two interstitials, Ultimate Tensile Strength increases, strain rate sensitivity becomes less negative and both strain hardening rate and tensile elongation decrease. On cold working with large strains, this is expected to have a positive influence; so carbon and nitrogen contents close to the upper limit of the ranges allowed by standards can be suggested.

5 REFERENCES

[1] S. Allain et al., Materials Science and Engineering A 387-389 (2004)158.

[2] F. Lecroisey, A. Pineau, Metallurgical Transactions 3 (1972) 387.

[3] P. Y. Volosevich et al., Physical Metallurgy and Metallography 42 (1976) 126.

[4] Y-K. Lee, C-S. Choi, Metallurgical and Materials Transactions 31A (2000) 355.

[5] P. J. Ferreira, P. Müllner, Acta Materialia 46(13) (1998) 4479.

[6] P. Müllner et al., Materials Science and Engineering A164 (1993) 164.

[7] R. E. Stolz, J. B. Vander Sande, Metallurgical Transactions 11A (1980) 1033.

[8] J. W. Simmons, Materials Science and Engineering A207 (1996) 159.

[9] J. W. Simmons, Acta Materialia 45(6) (1997) 2467.

[10] G. Saller et al., Materials Science and Engineering A427 (2006) 246.

[11] G. Krauss, Steels: Heat Treatment and Processing Principles, ed. Materials Park, Ohio, 1988.

[12] G. B. Olson, M. Cohen, Metallurgical Transactions 7A (1976) 1897.

[13] K. P. Staudhammer et al, Acta Metallurgica 31(2) (1983) 267.

[14] L. E. Murr et al., Metallurgical Transactions 13A (1982) 667.

[15] X. Tian, Y. Zhang, Materials Science and Engineering A174 (1994) L1.

[16] D. C. Ludwigson, Metallurgical Transactions 2 (1971) 2825.

[17] D. C. Ludwigson, J. A. Berger, Journal of The Iron and Steel Institute 207 (1969) 63.

[18] Y. G. Kim, C. Y. Lim, Metallurgical Transactions 19A (1988) 1625.

[19] A. A. Lebedev, V. V.Kosarchuk, International Journal of Plasticity 16 (2000) 749.

[20] A. K. De et al., Metallurgical and Materials Transactions 37A (2006) 1875.

[21] K. Spencer et al., Metarials Science and Engineering A387-389 (2004) 873.

[22] Z. Marciniak et al., Mechanics of Sheet Metal Forming, Butterworth-Heinemann, Oxford, 2002.

[23] H. Mancha et al., Journal of Materials Synthesis and Processing 4 (4) (1996) 217.